Advances in Science and Technology Research Journal

Advances in Science and Technology Research Journal, 2026, 20(6), 343–355
https://doi.org/10.12913/22998624/218094
ISSN 2299-8624, License CC-BY 4.0

Received: 2026.01.23
Accepted: 2026.04.15
Published: 2026.05.01

Cutting tool and workpiece deformation in friction drilling of aluminum alloy 6063 by finite element model simulation

Yogesh Ganpat Kamble[1*], Vipul Prabhakar Rathod[1], Rajiv B.[2], Prakash Pantawane[2], Sandeep H. Wankhade[3]

[1] Department of Robotics and Automation Engineering, D.Y. Patil College of Engineering, Akurdi, Pune, Maharashtra 411044, India
[2] Department of Manufacturing Science and Engineering, COEP Tech University Pune, Maharashtra 411005, India
[3] Department of Mechanical Engineering, AISSMS COE, Pune, Maharashtra 411001, India
* Corresponding author's e-mail: ygkamble@dypcoeakurdi.ac.in

ABSTRACT

Friction drilling is a non-traditional machining process widely used for creating holes in thin metallic sheets without material removal. The process involves severe plastic deformation at elevated temperatures, making it challenging to experimentally measure strain, stress, and deformation. To overcome this limitation, a finite element analysis (FEA) using ANSYS Explicit Dynamics was performed. A definitive screening design (DSD) with 13 runs was employed to investigate the effects of spindle speed, feed rate, workpiece thickness, and tool conical angle on process responses. Equivalent strain, equivalent stress, tool deformation, and workpiece deformation were analyzed across the simulation runs. The results indicate that equivalent strain and stress increase with spindle speed and feed rate, while deformation is primarily governed by workpiece thickness. This study demonstrates that DOE-based simulation provides a reliable framework for understanding complex thermo-mechanical behavior in friction drilling, enabling better tool design and process optimization.

Keywords: friction drilling, finite element analysis, ANSYS explicit dynamics, aluminum 6063-T6, simulation.

INTRODUCTION

Friction drilling is an advanced machining technique that utilizes heat generated by friction to soften and plastically deform material for hole formation [1]. Unlike conventional drilling, it avoids chip generation and improves material utilization, making it highly suitable for thin-walled components in automotive, aerospace, and structural applications [2,3].

The process involves high spindle speeds and localized thermal-mechanical interactions, leading to complex stress and strain distributions [4,5]. Direct measurement of these responses in experimental setups is difficult due to transient conditions and high-temperature gradients. Finite element analysis (FEA) provides an effective tool to model and simulate such processes, offering insights into strain, stress, and deformation mechanisms [6]. This work focuses on using ANSYS explicit dynamics to analyze the friction drilling process on aluminum alloy 6063-T6. A design of experiments (DOE) approach was integrated with the simulations to study the effects of multiple process parameters efficiently.

The effectiveness of friction drilling is strongly influenced by spindle speed, feed rate, and conical angle [7]. Multiple authors identify spindle speed and feed as the most critical determinants of hole quality [8]. Higher speeds enhance hole smoothness, while feed rate directly governs bush height and formation quality. For instance, thermal analyses revealed that materials with high conductivity and creep resistance respond more favorably, producing cleaner surface finishes [9,10]. On the contrary,

materials with poor thermal conductivity often fail to achieve sufficient softening, resulting in cracks or poor collar formation. In such cases, preheating has been recommended to improve ductility [11,12]. Investigations specifically on aluminum alloys such as Al 6063 and 6082 reported significant torque variations, ductility shifts, and instances of surface cracking at unfavorable feed-speed combinations [13]. Dynamometer studies emphasized that achieving dimensional accuracy requires careful balance between spindle speed, feed rate, and material thickness, as excessive heat zones lead to deformation [14].

Optimization of friction drilling parameters has received increasing attention in recent years. Methods combining Taguchi design, fuzzy logic, and multi-objective optimization have been applied to maximize bush height, minimize thrust force, and improve dimensional accuracy. For example, spindle speed, feed, and conical angle have been correlated with bush characteristics, demonstrating that a carefully balanced parameter set ensures superior hole formation and longer tool life [15,16]. This integration of computational modeling, FEM simulations, and experimental validation offers a comprehensive pathway to refining the process and adapting it for complex industrial applications.

Based on the reviewed literature, it is evident that friction drilling is dominated by complex, transient thermo-mechanical interactions at the tool–workpiece interface (Table 1). Building on these established findings, the present study focuses on numerically capturing the dynamic stress–strain–deformation behavior of AA6063 during friction drilling using an explicit FEM framework.

Tool and workpiece modeling

The geometries of plain and slotted center drill tools were modeled using CATIA V5 and imported into ANSYS Workbench. The workpiece was modeled as aluminum alloy 6063-T6 with defined elastic–plastic properties.

The process illustrated here represents the simulation of center drilling using ANSYS Explicit Dynamics (Table 2). Center drilling is an essential preparatory machining operation carried out to create a small, precise hole at the center of a workpiece. This hole serves as an accurate starting point for subsequent drilling or machining operations, ensuring alignment and minimizing tool deflection. The use of ANSYS Explicit Dynamics in this study is particularly important because it allows the capture of short-duration, transient phenomena that occur during high-speed machining. Unlike static analysis, explicit dynamics can simulate the complex interaction between the tool and the workpiece, making it possible to evaluate tool deformation, workpiece stress distribution, and elastic or plastic strain under different cutting conditions. By varying spindle speed and feed rate, the process behavior can be better understood, providing insight into optimizing machining parameters for improved performance and reduced tool wear. The selection of tool and workpiece size and geometry in the present study was guided by established friction drilling theory, reported experimental

Table 1. Experimentation and key findings [17–21]

Workpiece material	Focus / Method	Key findings / Phenomena
Various sheet metals	Experimental & thermal FEM (thrust force, torque, temperature)	Developed thermal and force models; heat generation & contact area control forces/temperature evolution.
Low carbon steel	Tool wear characterization	Tool wear quantified via mass/shape change; adhesive/oxidative/ abrasive wear observed; tool self-sharpening reduced thrust forces.
AISI 304	Taguchi experiments on process parameters	Optimal parameters (friction angle, feed, speed) found for surface finish; friction drill outperforming twist drill in durability.
Difficult-to-machine materials	Microstructure & tool wear review	High heat affects material properties and erosion; tool wear issues in friction drilling of challenging alloys.
Al7075-T651	Effect of pre-drilling geometry	Pre-drill depth/diameter influenced bushing shape and heat generation; reduced initiation deformation.
6082-T6 Aluminium	Mechanical properties & drilling speed	Identified optimal rotational speed range (3000–3500 rpm); localized hardening due to plastic work.
AISI 304/Al6061	Combined experimental & FEM joining study	Extended friction drilling to dissimilar joining; studied material flow and joint quality under thermo-mechanical conditions.
HX220 sheet	Meshless simulation study	Smoothed Particle Galerkin method for material flow, axial force, torque, and temperature modelling; an alternative to traditional FEM.

Table 2. Properties of workpiece material

Property	Mean value	Standard deviation (±)	Unit
Density	2700	20	kg/m³
Young's modulus	68.9	2	GPa
Poisson's ratio	0.33	0.01	–
Yield strength (0.2% offset)	214	8	MPa
Ultimate tensile strength	241	10	MPa
Elongation at break	12	1.5	%
Hardness (HBW)	73	4	HB
Thermal conductivity	201	8	W/m·K
Specific heat capacity	900	30	J/kg·K
Coefficient of thermal expansion	23.5×10^{-6}	0.7×10^{-6}	1/K
Flow stress (at elevated temp.)	Temperature-dependent	—	MPa

practices, and numerical modeling requirements to ensure realistic representation of tool–workpiece interaction. Friction drilling is fundamentally governed by tool geometry, particularly the conical angle and cylindrical land, which control frictional heat generation, material softening, and subsequent plastic flow of the workpiece material. Previous studies have demonstrated that conical tools with included angles typically ranging between 30° and 60° promote stable heat generation and uniform bushing formation in aluminum alloys, while minimizing excessive thrust force and tool wear. Accordingly, a standard friction drilling tool profile consisting of a conical entry region followed by a cylindrical section was adopted in the present FEM model to reflect industrially accepted practice and widely reported literature configurations.

The primary reason for opting for Ansys explicit dynamic is that it suits to capture the physics of short duration while operating for products that sometimes undergo transient dynamic forces. The deformation of the tool and workpiece, equivalent stress, and plastic strain of the process with varying spindle speed and feed simulate explicit dynamics. Mentioned exploratory experiments are used for three different geometry of center drill tools.

In explicit dynamic simulations, the reported total deformation includes both elastic–plastic deformation and elastic body motion of unconstrained nodes. Therefore, absolute deformation values are not directly interpreted as physical dimensional changes. To ensure physical relevance, deformation analysis was focused on localized displacement at the tool–workpiece contact zone, while suppressing global elastic body motion effects. The friction drilling tool was modeled as an elastic body to capture relative deformation trends under varying process parameters. However, due to the significantly higher stiffness of the tool compared to the aluminum workpiece, tool deformation results are interpreted qualitatively.

Dynamic behavior of tool-workpiece interaction in friction drilling

Friction drilling is a highly transient thermomechanical process characterized by continuously evolving thrust force, tool velocity, contact duration, and deformation rate. Unlike conventional drilling, where cutting mechanics dominate, friction drilling relies on frictional heating and severe plastic deformation, making dynamic response a governing factor. Literature consistently reports that the process dynamics evolve through distinct stages, each associated with different force, velocity, temperature, and deformation characteristics. Thermal effects are incorporated implicitly through temperature-dependent material properties calibrated from literature.

Stages of dynamic interaction

Stage I: Initial tool-workpiece contact

At the onset of drilling, the rotating conical tool makes contact with the workpiece surface, resulting in a rapid rise in thrust force due to elastic resistance of the material. The relative sliding velocity at the interface generates frictional heat, but material flow is minimal at this stage.

Stage II: Thermally assisted plastic deformation

As drilling progresses, frictional heat accumulation elevates the local temperature near the

tool–workpiece interface. Literature shows that once the temperature approaches a critical fraction of the alloy's melting temperature, thermal softening dominates, reducing flow stress. Consequently, thrust force stabilizes or slightly decreases despite increasing penetration depth.

Stage III: Material flow and bushing formation

In the final stage, softened material flows axially and radially to form a bushing. The contact duration increases significantly, and thrust force reaches a quasi-steady or peak-limited value (Table 3).

Time-dependent thrust force evolution

The thrust force in friction drilling is not constant and evolves dynamically with penetration depth and temperature. Literature reports a characteristic force-time curve consisting of an initial sharp rise, followed by stabilization and eventual reduction as thermal softening dominates. The FEM results capture this behavior by resolving force response at each time increment. Higher spindle speeds reduce peak thrust force due to enhanced thermal softening, while higher feed rates increase thrust due to elevated strain rate effects (Table 4).

Velocity and strain rate effects

Tool velocity directly influences strain rate, which in turn affects flow stress under high-temperature conditions. Literature consistently indicates that aluminum alloys exhibit strain rate sensitivity during friction drilling, especially under elevated temperatures. The present model incorporates velocity-dependent material behavior using temperature-dependent plasticity models.

Contact duration and thermal accumulation

Contact duration is a critical yet often overlooked parameter. Longer tool–workpiece contact allows greater heat accumulation, enhancing thermal softening but increasing risk of excessive tool deformation. Studies emphasize that optimal contact duration balances heat generation with material flow stability. The FEM model tracks contact time at the interface, enabling correlation between duration, temperature rise, and deformation extent (Table 5, Figure 1).

The outlines the process parameters selected for conducting exploratory experiments in the center drilling study. Four input variables were considered critical for understanding the machining behavior spindle speed, feed rate, material thickness, and the conical angle of the tool. Each of these parameters was varied at three levels, namely lower, middle, and higher, to represent a wide operating window. Spindle speed was set at 2000, 4000, and 6000 rpm to study how changes in cutting velocity influence heat generation, chip formation, and stress levels in the workpiece. Feed rate was chosen at 45, 60, and 75 mm/min, since this parameter directly affects the material removal rate, surface finish, and tool load. Material thickness was varied between 1.5, 2.25, and 3 mm to simulate the response of thin, medium, and thick sections during drilling. Lastly, the conical angle of the tool was set at 36°, 39°, and 42°, since

Table 3. Dynamic process parameters considered in the FEM model

Parameter	Range / Description	Literature basis
Tool rotational speed	Variable (DOE-based)	Controls frictional heat generation
Feed velocity	Variable (DOE-based)	Governs strain rate and thrust force
Contact duration	Time-dependent	Influences heat accumulation
Thrust force	Transient response	Peak force linked to thickness
Acceleration	Non-uniform	Affects dynamic stability

Table 4. Typical thrust force trends observed in literature and FEM

Process stage	Thrust force trend	Governing mechanism
Initial contact	Rapid increase	Elastic–plastic resistance
Mid-penetration	Stabilization	Thermal softening
Bushing formation	Gradual decrease / steady	Material flow dominance

Table 5. Influence of contact duration on deformation behavior

Velocity increase	Observed effect	Literature observation
Low → Moderate	Increased heat, reduced force	Stable deformation
Moderate → High	Reduced force, higher strain	Uniform bushing
Excessively High	Tool wear risk	Interface instability

Table 6. Parameters to conduct exploratory experiments

Parameters	Lower	Middle	Higher
Spindle speed in rpm	2000	4000	6000
Feed-in mm/min	45	60	75
Material thickness in mm	1.5	2.25	3
The conical angle of the tool	36°	39°	42°

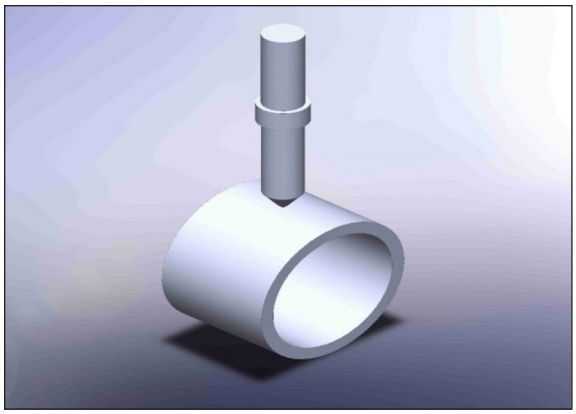

Figure 1. Model of center drill and workpiece

tool geometry plays an important role in determining the cutting edge engagement, penetration efficiency, and stress concentration at the drill tip.

Studying four parameters at three levels each would require 81 simulations in a full factorial design. However, such an approach would be computationally expensive and impractical for detailed FEM analysis. Therefore, a Definitive Screening Design with 13 runs was selected, as it efficiently captures the most influential parameters and their nonlinear trends with far fewer simulations. This design is well suited for friction drilling, where responses are highly nonlinear, and it provides reliable insights while significantly reducing time and computational cost (Table 6).

PROCEDURE TO PERFORM SIMULATION ON CENTER DRILL TOOL AND WORKPIECE

Equivalent stress, strain, and deformation of tool and workpiece simulates 13 experimental runs; the mentioned experiments use a definitive screening design method. An initial experimental run is done using workpiece material thickness

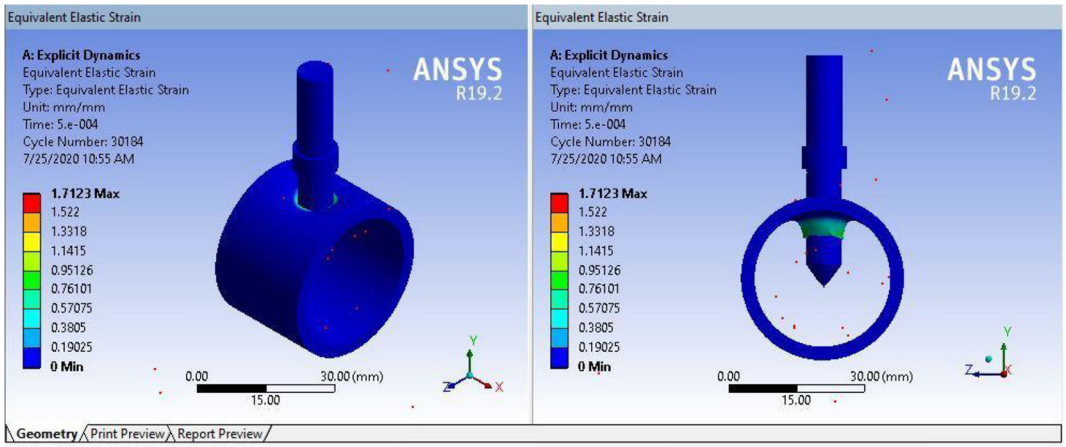

Figure 2. Equivalent plastic strain

as 3 mm, 75 mm/min feed, and 2000 rpm as the spindle speed. The simulation of the exploratory experiments utilized to know the phenomenon like equivalent plastic strain in friction drilling, which elaborates for the strain until the center drill tool material and workpiece material has to rebound and come back to their original shape once the removal of the load.

Figure 2 shows the distribution of equivalent plastic strain in the workpiece during the center drilling process, obtained through ANSYS Explicit Dynamics. The color scale indicates the magnitude of strain, where red zones correspond to higher strain concentration and blue zones indicate minimal strain. From the simulation, it is evident that the maximum strain (1.7123 mm/mm) occurs near the cutting zone, where the drill tip makes initial contact with the workpiece surface. This is expected, as the tool penetrates into the material, creating localized stresses that translate into strain. The rest of the workpiece experiences much lower strain, remaining largely in the elastic zone. This result highlights how drilling parameters, such as feed rate and spindle speed, primarily affect the localized region of the tool–workpiece interface.

The equivalent plastic strain distribution illustrates the extent of irreversible deformation occurring during friction drilling. High strain values (1.7–2.8 mm/mm) near the tool–workpiece interface confirm dominance of plastic flow, which is essential for bushing formation.

Figure 2 illustrates the equivalent von-Mises stress distribution in the workpiece during drilling. Von-Mises stress is widely used in engineering analysis to evaluate whether the material will yield under complex loading conditions. The simulation reveals that stress is highly concentrated near the contact region between the tool tip and the workpiece. The maximum stress observed is about 315.71 MPa, which occurs at the drilling interface. As expected, regions away from the contact zone show much lower stress values, confirming that the drilling process mainly influences the immediate cutting region.

Figure 3 presents the total deformation of the plain center drill tool during operation. Deformation here refers to the displacement experienced by the tool under cutting forces, measured in millimeters. The simulation results indicate a maximum deformation of 22.014 mm, concentrated near the tool tip and shaft interface. This suggests that the highest bending or deflection occurs where the tool engages with the workpiece, while the shank experiences minimal displacement. Although elastic deformation of the tool is unavoidable, excessive values may affect hole accuracy, surface quality, and tool life. By analyzing this deformation behavior, one can assess the rigidity of the tool design and the suitability of machining parameters. Optimizing spindle speed, feed rate, and tool geometry can significantly reduce deformation, leading to better precision and longer tool performance.

The reported von Mises stress values exceed the room-temperature ultimate tensile strength of AA6063-T6. This is attributed to severe plastic deformation under high strain rate and confined contact conditions inherent to friction drilling. In the absence of a damage or failure model, these stress values represent instantaneous flow stress rather than failure stress. Therefore, the stress results are

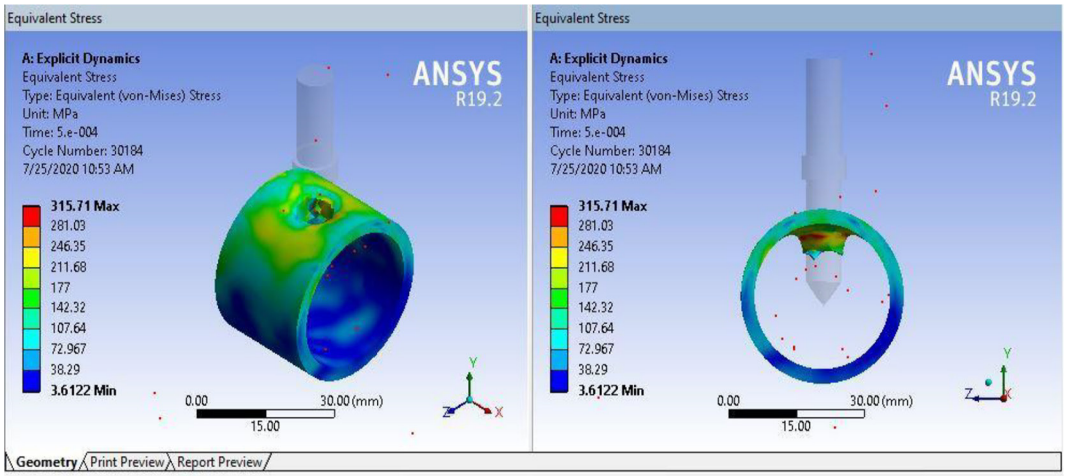

Figure 3. Equivalent stress

interpreted comparatively to assess parameter influence, not to predict material fracture.

After that, in Figure.4, total deformation of center drill is observed as tool deformation take places through the workpiece material is to be analyzed in all directions viz. X, Y, and Z direction. Above Figure. shows workpiece material AL 6063 deformation for 22.014 mm. The color scale represents relative displacement fields amplified by dynamic motion and should not be interpreted as true dimensional change.

The deformation contours primarily indicate displacement trends rather than absolute dimensional changes. The maximum deformation values represent cumulative displacement due to dynamic motion of the tool, while localized deformation near the tool tip governs machining accuracy.

In the isometric view (left side), the workpiece is shown as a cylindrical component subjected to tool interaction. The deformation is represented using a color contour scale ranging from deep blue (indicating minimum deformation) to bright red (indicating maximum deformation). The scale on the left specifies the deformation values in millimeters, with the maximum reaching about 219.66 mm. The contour reveals that the majority of the workpiece remains relatively stable (in darker blue shades), while localized regions near the tool contact experience the most significant deformation, indicated by red and orange areas. This highlights that the deformation is concentrated where the tool engages the material, which is expected in machining simulations.

The sectional view (right side) further clarifies the internal distribution of deformation. By cutting through the middle of the workpiece, this view shows how the deformation propagates from the cutting zone into the surrounding material. The inner region near the tool shows maximum deformation (red zones), while areas away from the contact surface remain largely undeformed (blue regions). This visualization helps in understanding the depth of deformation penetration and its effect on the internal structure of the workpiece.

Tool–workpiece interaction induces high localized deformation, with the highest stress and strain concentration occurring in the tool contact region. Such results are crucial in machining simulations because they indicate potential zones of material failure, residual stress development, and dimensional inaccuracies. Engineers and researchers use this type of analysis to optimize cutting parameters, tool design, and workpiece material selection to minimize excessive deformation and improve machining performance.

As with the deformation of the center drill, workpiece deformation is vital in the friction drilling process (Figure 5). Although large numerical displacement values are observed, the physically meaningful deformation is confined to the immediate contact region. The results are therefore used for comparative trend analysis across parameter combinations rather than absolute magnitude interpretation. Table 7 presents the simulated FEM results obtained from ANSYS, showing how variations in machining parameters such as material thickness, spindle speed, tool angle, and feed rate affect strain, stress, and the deformation of both the tool and the workpiece. Each run represents a different set of input conditions, and the outputs provide a clear picture of the mechanical behavior of the system during the cutting process.

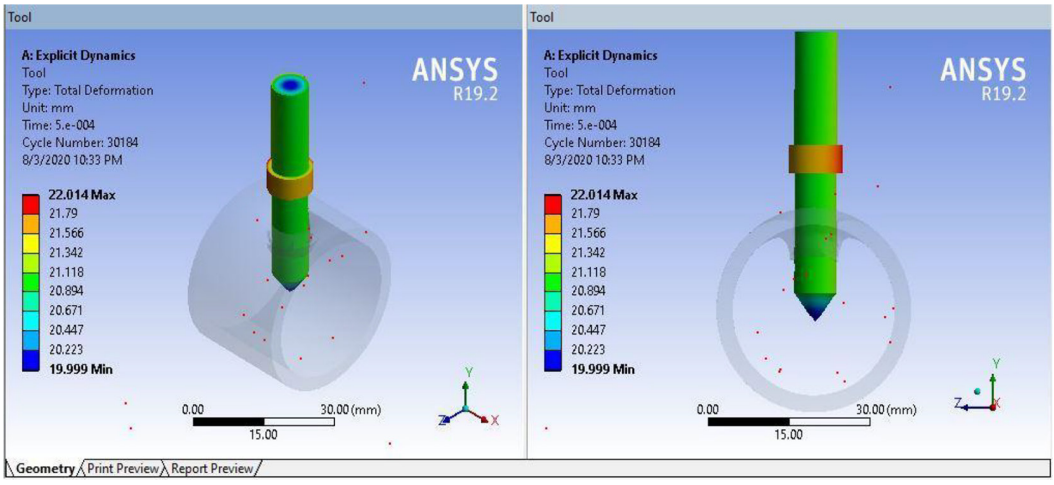

Figure 4. Total deformation of the plain center drilling tool

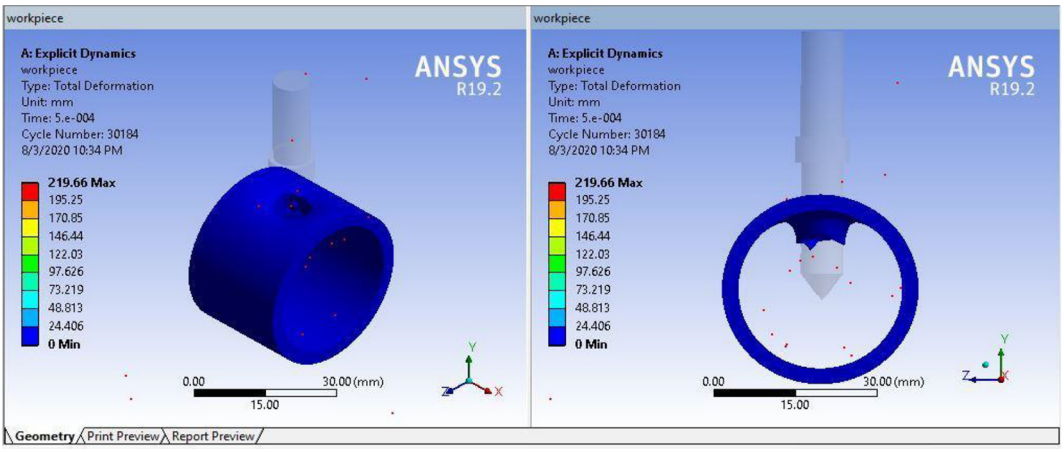

Figure 5. Total workpiece deformation

Table 7. Simulated FEM results by Ansys

Run order	Material thickness	Speed	Angle	Feed	Equivalent plastic strain	Stress	Relative tool displacement (trend indicator)	Relative workpiece displacement
	mm	RPM	Degree	mm/min	(mm/mm)	MPa	mm	mm
1	3	2000	36	75	1.7123	315.71	22.014	19.66
2	3	4000	36	45	1.4557	341.76	22.012	19.62
3	3	6000	42	60	2.2274	427.83	20.092	25.085
4	1.5	4000	42	75	2.0426	426.38	21.114	23.807
5	3	2000	42	45	1.314	309.89	21.805	29.279
6	1.5	2000	36	60	0.86099	308.84	21.809	24.793
7	3	6000	39	75	1.9321	427.45	15.069	10.78
8	1.5	6000	36	75	2.7892	488.42	12.606	28.818
9	2.25	2000	42	75	2.2087	398.86	19.521	22.994
10	2.25	6000	36	45	1.3586	296.98	20.109	29.38
11	1.5	6000	42	45	1.3927	632.77	7.0739	14.403
12	15	2000	39	45	1.5582	328.28	19.521	26.783
13	2.25	4000	39	60	2.1181	423.9	21.473	21.473

From the results, it can be observed that the strain values vary considerably across different runs, ranging from 0.86 mm/mm to 2.78 mm/mm. Lower strain values are recorded when the cutting is performed at lower spindle speeds and larger material thicknesses, whereas higher strain values are linked to higher cutting speeds and thinner materials. This indicates that as the intensity of machining increases, the workpiece undergoes greater plastic deformation. The stress response shows a similar trend, with values spanning from 296.98 MPa to 632.77 MPa. Higher stresses are observed under high-speed cutting conditions and smaller material thicknesses. For instance, Run 11 records the maximum stress of 632.77 MPa, which corresponds to thinner material and higher speed, highlighting the fact that thinner workpieces experience higher localized stresses as they resist material removal. Such conditions may accelerate tool wear and negatively impact the surface finish.

Tool deformation is relatively stable compared to workpiece deformation, with most values lying between 15 mm and 22 mm. However, some extreme cases, such as Run 11, show a minimum tool deformation of 7.07 mm despite very high stress, suggesting that the deformation of the tool is not always directly proportional to the applied stress but also influenced by geometry and material behavior. Generally, thicker workpieces and lower spindle speeds result in greater tool

deformation, while thinner materials and higher speeds tend to reduce tool displacement.

Workpiece deformation exhibits the widest variation, ranging from 10.78 mm to 50.08 mm. Higher deformations are observed at higher spindle speeds and moderate thicknesses, such as Run 3, where the workpiece deformation reaches 50.08 mm at 6000 RPM. This indicates that aggressive machining conditions can severely distort the workpiece, affecting dimensional accuracy and leading to possible rejection in precision manufacturing processes. On the other hand, lower deformation values are achieved under balanced speed and feed conditions, as seen in Run 7.

From the results, it can be concluded that machining at moderate spindle speeds (around 2000–4000 RPM) with controlled feed rates provides a better balance between tool and workpiece deformation. Extremely high speeds and thin material sections tend to increase stress and workpiece deformation significantly, whereas lower speeds and thicker sections cause higher tool deformation. Hence, selecting an optimum mid-range speed and feed combination is crucial for minimizing overall deformation and achieving stable machining performance.

Experimental confirmation of FEM results

In the validation of the developed finite element (FEM) model, selected friction drilling experiments were conducted under representative combinations of spindle speed, feed rate, workpiece thickness, and tool tip angle. Since direct experimental measurement of equivalent stress and equivalent strain is impractical in friction drilling due to severe plastic deformation and high localized temperatures, experimentally measurable responses namely thrust force, bush length, hole size, and bush quality were used as indirect indicators of FEM-predicted stress–strain-deformation behavior.

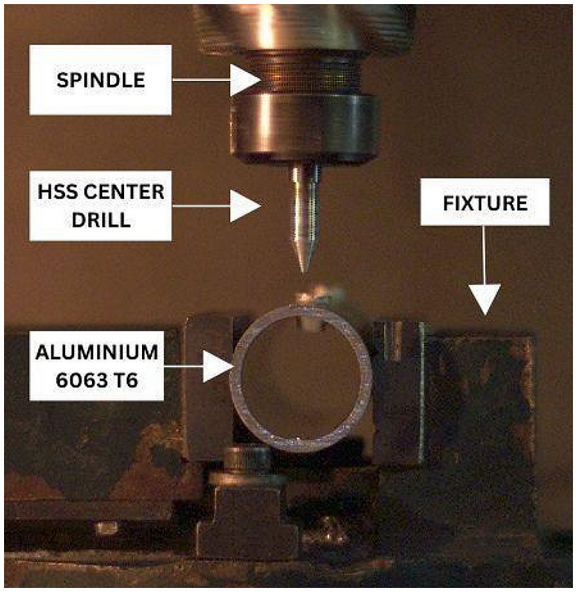

Figure 6. Experimental setup

For the confirmation experiments, a high speed steel (HSS) center drill conforming to ASTM 600 was selected as the friction drilling tool, owing to its balanced combination of hardness, toughness, thermal stability, and cost effectiveness. The tool material, enriched with alloying elements such as carbon, chromium, molybdenum, tungsten, and vanadium, provides adequate wear resistance and strength to withstand the severe thermo-mechanical loading associated with friction drilling. A controlled heat treatment involving preheating, austenitizing, quenching, and tempering was employed to achieve a hardened martensitic microstructure with a final hardness of approximately 55–58 HRC, ensuring consistent tool performance during experimentation. Aluminium alloy 6063 tubes of varying thickness were selected as the workpiece material due to their widespread industrial use, favorable strength-to-weight ratio, good formability, and thermal conductivity. These characteristics make AA6063 particularly suitable for friction drilling, allowing stable plastic deformation and reliable bush formation, thereby enabling effective experimental validation of the FEM-predicted stress, strain, and deformation behavior.

It is acknowledged that direct experimental measurement of stress and strain is not feasible in friction drilling. Therefore, validation is limited to indirect indicators such as thrust force, bush length, and hole quality, and is qualitative in nature. Table 8 and Figure 6 presents the experimental results corresponding to four representative runs. A strong qualitative agreement is observed between FEM predictions and experimental outcomes across all cases.

Correlation between FEM stress and experimental thrust force

The FEM simulations predicted that equivalent stress is primarily influenced by workpiece thickness and feed rate, while increasing spindle

Table 8. Experimental conformation results

Run	Tip angle (°)	Speed (rpm)	Feed (mm/min)	Thickness (mm)	Thrust force (N)	Hole size (mm)	Bush length (mm)
1	39	2000	50	1.5	800.1	7.92	3.3
2	39	4000	65	2.25	828.3	8.07	4.9
3	39	6000	65	3	827.1	7.921	6.6
4	39	6000	80	2.25	823.84	8.105	4.5

speed induces thermal softening, thereby limiting excessive stress rise. This trend is experimentally confirmed by the thrust force values listed in Table 9. Despite a substantial increase in spindle speed from 2000 rpm to 6000 rpm, the thrust force remains within a narrow range (approximately 800–828 N), indicating effective thermal softening of the material at higher speeds.

The slightly higher thrust force observed for increased thickness (2.25–3 mm) supports the FEM prediction that thicker workpieces offer greater resistance to deformation due to increased material volume participating in plastic flow. Thus, the experimental thrust force behavior validates the FEM-predicted stress distribution and load transfer mechanism during friction drilling.

Correlation between FEM strain and bush length formation

Equivalent strain obtained from FEM simulations represents the extent of plastic deformation and material flow responsible for bush formation. Experimentally, this deformation is directly reflected in bush length and bush quality. As shown in Table 9, bush length increases significantly with increasing workpiece thickness and spindle speed.

For Run 1 (1.5 mm thickness, 2000 rpm), limited bush formation 3.3 mm with moderate quality was observed, indicating restricted plastic flow consistent with FEM results showing lower equivalent strain under such conditions. In contrast, Run 3 (3 mm thickness, 6000 rpm) produced the longest bush 6.6 mm with excellent quality, confirming FEM-predicted high equivalent strain and stable material flow at elevated temperature and sufficient thickness.

The close agreement between predicted strain trends and experimentally measured bush length confirms the FEM model's capability to accurately capture plastic flow behavior during bushing formation.

Effect of feed rate on deformation stability

The FEM analysis indicated that while higher feed rates increase deformation intensity, excessive feed can reduce deformation stability by limiting heat accumulation and material flow time. This phenomenon is experimentally evident when comparing Runs 2 and 4, both conducted at similar thickness but different feed rates. Run 4 operated at high spindle speed, the increased feed rate resulted in reduced bush length and only fair bush quality compared to Run 2. This behavior confirms FEM-predicted deformation instability at higher feed rates, where non-uniform strain distribution leads to inferior bush formation despite sufficient thermal input.

Hole size and overall deformation consistency

Hole size measurements further support FEM predictions of total deformation behavior. Conditions associated with stable deformation and higher strain (Runs 2 and 3) produced hole sizes closer to the nominal value with better bush integrity, whereas unstable deformation conditions resulted in greater dimensional variation. This confirms that FEM-predicted deformation uniformity directly influences final hole geometry and quality.

Overall validation of FEM model

The experimental results show strong agreement with FEM predictions in terms of stress trends, strain-driven bush formation, deformation stability, and geometric accuracy. The experimentally observed thrust force, bush length, and bush quality consistently follow the trends predicted by equivalent stress, equivalent strain, and deformation fields obtained from FEM simulations. FEM-experimental correlation confirms that the developed numerical model accurately represents the thermo-mechanical behavior of friction drilling and can be reliably used for process

analysis, optimization, and parameter selection with reduced experimental effort.

Grey relational analysis

Grey relational analysis (GRA) is a multi-criteria decision-making technique used to evaluate and rank experimental trials when multiple performance measures must be considered simultaneously. In the present friction drilling study, the key output parameters are strain, stress, tool deformation, and workpiece deformation. Normalized trends were used to rank parameter combinations based on relative deformation severity rather than absolute desirability of individual responses. The normalized values are then compared against the ideal reference sequence (which is always 1), and the deviation sequence is calculated to measure how far each trial is from the ideal case. From these deviations, the grey relational coefficients (GRC) are derived, which indicate the closeness of each trial to the ideal solution. Finally, the grey relational grade (GRG) is obtained by averaging the coefficients of all responses for each experiment, and this grade represents the overall performance index. The trial with the highest GRG is considered the optimal parameter setting, as it best satisfies all the performance requirements collectively. In this way, GRA provides a systematic and effective approach to identify the most suitable process conditions in friction drilling by balancing multiple quality indicators.

Table 9. Deviation sequence and global Δmin and Δmax

Normalization (lower is better)				Calculate Δ (absolute difference from ideal = 1)			
0.558	0.944	0.000	0.523	0.442	0.056	1.000	0.477
0.692	0.867	0.000	0.525	0.308	0.133	1.000	0.475
0.291	0.610	0.129	0.231	0.709	0.390	0.871	0.769
0.387	0.615	0.060	0.300	0.613	0.385	0.940	0.700
0.765	0.962	0.014	0.005	0.235	0.038	0.986	0.995
1.000	0.965	0.014	0.247	0.000	0.035	0.986	0.753
0.445	0.611	0.465	1.000	0.555	0.389	0.535	0.000
0.000	0.430	0.630	0.030	1.000	0.570	0.370	0.970
0.301	0.697	0.167	0.343	0.699	0.303	0.833	0.657
0.742	1.000	0.128	0.000	0.258	0.000	0.872	1.000
0.724	0.000	1.000	0.805	0.276	1.000	0.000	0.195
0.638	0.907	0.167	0.140	0.362	0.093	0.833	0.860
0.348	0.622	0.036	0.425	0.652	0.378	0.964	0.575

Table 10. Calculating rank from grey relational grade

Grey relational coefficients (GRC)		Grey relational grade (GRG)		Rank	
0.531	0.900	0.333	0.512	0.569	6
0.618	0.789	0.333	0.513	0.563	7
0.414	0.562	0.365	0.394	0.434	12
0.449	0.565	0.347	0.417	0.444	11
0.680	0.929	0.336	0.335	0.570	5
1.000	0.934	0.336	0.399	0.667	2
0.474	0.563	0.483	1.000	0.630	3
0.333	0.467	0.575	0.340	0.429	13
0.417	0.622	0.375	0.432	0.462	9
0.660	1.000	0.364	0.333	0.589	4
0.645	0.333	1.000	0.720	0.674	1
0.580	0.843	0.375	0.368	0.541	8
0.434	0.569	0.342	0.465	0.453	10

Grey relational analysis was applied to normalized FEM outputs to evaluate relative performance trends across experimental runs. Since absolute magnitudes may be affected by modeling assumptions, normalization ensures that ranking is governed by comparative behavior rather than numerical scale.

The present FEM model does not incorporate material damage, fracture, or element deletion criteria. Hence, stress magnitudes are interpreted as relative indicators of process severity rather than absolute failure thresholds (Table 10).

CONCLUSIONS

FEM results confirm that spindle speed and workpiece thickness are the most dominant parameters influencing strain, stress, and deformation during friction drilling. The FEM results indicate that spindle speed and workpiece thickness are the most influential parameters governing strain, stress, and deformation behavior during friction drilling of AA6063. The numerical analysis demonstrates that process responses are governed by the combined interaction of multiple parameters rather than by isolated effects.

A balanced operating window in the range of 2000–4000 rpm spindle speed and 45–60 mm/min feed rate was identified as providing a favorable compromise between tool stability, stress concentration, and workpiece deformation. Grey Relational Analysis proved effective in simultaneously optimizing multiple performance measures, with Run 11 yielding the highest overall performance index under the selected criteria.

The FEM-predicted trends of stress and strain showed good qualitative agreement with experimental observations in terms of thrust force, bush length, and bush quality, confirming the capability of the model to capture dominant deformation mechanisms. The study demonstrates that an explicit dynamic FEM framework combined with a reduced experimental design can reliably capture key friction drilling trends and support preliminary process optimization with reduced experimental effort.

REFERENCES

1. Miller, S. F., Tao, J., Shih, A. J. Friction drilling of cast metals. International Journal of Machine Tools and Manufacture, 2006; 46(12–13), 1526–1535, https://doi.org/10.1016/j.ijmachtools.2005.09.003
2. Lee, S. M., Chow, H. M., Huang, F. Y., Yan, B. H. Friction drilling of austenitic stainless steel by uncoated and PVD AlCrN- and TiAlN-coated tungsten carbide tools, International Journal of Machine Tools & Manufacture 2009; 49, 81–88, https://doi.org/10.1016/j.ijmachtools.2008.07.012
3. El-Bahloul, S. A., El-Shourbagy H. E. and El-Midany, T. T. Optimization of thermal friction drilling process based on taguchi method and fuzzy logic technique, International Journal of Science and Engineering Applications, 2015; 4(2), http://dx.doi.org/10.7753/IJSEA0402.1006
4. Schulze, V. F., Zanger, J. M., Lang, F. 3D-FE-Modelling of the Drilling Process – Prediction of Phase Transformations at the Surface Layer, 14th CIRP Conference on Modeling of Machining Operations, Procedia CIRP 2013; 8, 33–38, https://doi.org/10.1016/j.procir.2013.06.061
5. Pantawane P.D., Ahuja. B.B., Experimental investigations and multi-objective optimization of friction drilling process on AISI 1015, International Journal of Applied Engineering Research, Dindigul, 2011; 2(2).
6. Dehghan, S., Soury, E. A comparative study on machining and tool performance in friction drilling of difficult-to-machine materials AISI 304, Ti-6Al-4V, Inconel 718. Journal of Manufacturing Processes, 2021; 61, 128–152, http://dx.doi.org/10.1016/j.jmapro.2020.10.078
7. Dehghan, S., Ismailia, S. M. I., Souri, E. A thermo-mechanical finite element simulation model to analyze bushing formation and drilling tool for friction drilling of difficult-to-machine materials, Journal of Manufacturing Processes 2020; 57, 1004–1018, http://dx.doi.org/10.1016/j.jmapro.2020.07.022
8. Alphonse, M. Raja, V. B., Palanikumar, K, Sanjay, D.S.K., Subbaiah, B.V., Chandra, L.V Highlights of Non-traditional friction drilling process: A review. Materials Today: Proceedings, 2021. http://dx.doi.org/10.1016/j.matpr.2021.01.336
9. Miller, S. F., Blau, P. J. and Shih, A. J. Tool wear in friction drilling. International Journal of Machine Tools and Manufacture 2007; 47(10): 1636–1645, https://doi.org/10.1016/j.ijmachtools.2006.10.009
10. Scott F. Miller, Peter J. Blau, and Albert J. Shih, Microstructural alterations associated with friction drilling of steel, aluminum, and titanium, JMEPEG 2005; 14: 647–653, http://dx.doi.org/10.1361/105994905X64558
11. Potdar, A., Sapkal, S. (2020). Optimization of friction drilling process by response surface methodology. In Advanced Engineering Optimization through Intelligent Techniques 351–359. Springer, Singapore, http://dx.doi.org/10.1007/978-981-13-8196-6_31
12. Mustafa, Z., Idrus, N. H., Hadzley, A. B. M., Sivakumar, D., Norazlina, M. Y., Fadzullah, S. H. S.

M., Thongkaew, K. Optimization of drilling process parameters on delamination factor of Jute reinforced unsaturated polyester composite using Box-Behnken design of experiment. Journal of Mechanical Engineering and Sciences, 2020; 14(1), 6295–6303, https://doi.org/10.15282/jmes.14.1.2020.08.0493

13. Ku, W.-L., Hung, C.-L., Lee, S.-M., Chow, H.-M. Optimization in thermal friction drilling for SUS 304stainless steel International Journal Advanced Manufacturing Technology 2011; 53, 935–944, http://dx.doi.org/10.1007/s00170-010-2899-5
14. Chow, H.-M., Lee, S.-M., Yang, L.-D. Machining characteristic study of friction drilling on AISI 304 stainless steel. Journal of materials processing technology 2008; 207. https://doi.org/10.1016/j.jmatprotec.2007.12.064
15. Agarwal, G., and Khare, M. K. Multi objective optimization of cutting parameters in machining–a sustainable approach. Materials Today: Proceedings 2020, https://doi.org/10.1016/j.matpr.2020.09.272
16. Kaviarasan, V., Venkatesan, R. and Natarajan, E. Prediction of surface quality and optimization of process parameters in drilling of Delrin using neural network. Progress in Rubber, Plastics and Recycling Technology 2019; 35(3), 149–169, https://doi.org/10.1177/1477760619855078
17. Selvaraj, R. M., and Rajesh, N., Hynes, J. Finite element approach in thermal modelling of friction stud welding. In AIP Conference Proceedings, 2019; 2142(1), 110006. AIP Publishing LLC, https://doi.org/10.1063/1.5122466
18. Sharma, V. K., Kumar, V., Joshi, R. S. and Sharma, D. Experimental analysis and characterization of SiC and RE oxides reinforced Al-6063 alloy based hybrid composites. The International Journal of Advanced Manufacturing Technology 2020; 108(4), 1173–1187.
19. Skovron, J. D., Prasad, R. R., Ulutan, D., Mears, L., Detwiler, D., Paolini, D., Baeumler, B. and Claus, L. Effect of thermal assistance on the joint quality of Al6063-T5A during flow drill screw driving. Journal of Manufacturing Science and Engineering 2015; 137, 5.
20. Kamble, Y., Rajiv, B. Experimental investigation and dimensional analysis of friction drilled hole on 6082 aluminium pipe using hardened M2 centre drill,Materials today proceedings, 2021; 42, Part 2, 1239–1243, http://dx.doi.org/10.1016/j.matpr.2020.12.874
21. Kamble, Y.G., Pantawane, P.D., Rajiv, B., Ahuja, B.B. Design and Development of Combination Tool for Drilling and Tapping Operation on PVC. In: Shunmugam, M., Kanthababu, M. (Eds) Advances in Simulation, Product Design and Development. Lecture Notes on Multidisciplinary Industrial Engineering. Springer, Singapore. 2020. https://doi.org/10.1007/978-981-32-9487-5_44
22. Rathod, V. P., Wankhade, S. H. A review on impact of micro-tools on micro-milling outcomes for aluminium alloy. Advances in Science and Technology Research Journal, 2025; 19(3), 322–340. https://doi.org/10.12913/22998624/200007
23. Rathod, V. P., Wankhade, S. H. Comprehensive review of tool treatments and innovations in micro-milling precision and performance. Advances in Science and Technology Research Journal, 2025; 19(4), 241–257. https://doi.org/10.12913/22998624/200545
24. Rathod, V. P., Wankhade, S. H., Kamble, Y. G. (2025). Evaluating the efficiency of micro end mill tools and performance metrics in micro milling. Journal of Mines, Metals and Fuels, 73(7), 2253–2265. https://doi.org/10.18311/jmmf/2025/49414
25. Kamble, Y. G., B., R., Rathod, V. P., Pantawane, P., Wankhade, S. (2025). Center drill geometry mapping in friction drilling of aluminium 6063 using artificial neural network approach. Advances in Science and Technology Research Journal, 19(11), 124–148. https://doi.org/10.12913/22998624/209120
26. Rathod VP, Wankhade SH, Kamble YG. Experimental analysis of process parameters in micro-milling of AA6063-T6 using 7% cobalt WC tools. Advances in Science and Technology Research Journal. 2026;20(1), https://doi.org/10.12913/22998624/210942